Smectic-*A* elastomers with weak director anchoring

J. M. Adams and Mark Warner

Cavendish Laboratory, JJ Thomson Avenue, Cambridge CB3 0HE, United Kingdom

Olaf Stenull and T. C. Lubensky

Department of Physics and Astronomy, University of Pennsylvania, Philadelphia, Pennsylvania 19104, USA

Experimentally it is possible to manipulate the director in a (chiral) smectic-*A* elastomer using an electric field. This suggests that the director is not necessarily locked to the layer normal, as described in earlier papers that extended rubber elasticity theory to smectics. Here, we consider the case that the director is weakly anchored to the layer normal assuming that there is a free energy penalty associated with relative tilt between the two. We use a recently developed weak-anchoring generalization of rubber elastic approaches to smectic elastomers and study shearing in the plane of the layers, stretching in the plane of the layers, and compression and elongation parallel to the layer normal. We calculate, inter alia, the engineering stress and the tilt angle between director and layer normal as functions of the applied deformation. For the latter three deformations, our results predict the existence of an instability towards the development of shear accompanied by smectic-*C*-like order.

PACS number(s): 61.30.Vx, 83.80.Va, 81.40.Jj

I. INTRODUCTION

Smectic-*A* (Sm-*A*) liquid crystal elastomers incorporate the anisotropic properties of liquid crystals, and the rubber elasticity of polymer networks. The formation of a smectic layer structure by the mesogens is the cause of their particularly anisotropic elastic properties. These elastomers have been synthesized, and their elastic properties explored through mechanical testing. Nishikawa and Finkelmann found that a class of strongly coupled Sm-*A* systems behave like two-dimensional (2D) elastomers in the layer plane [1] but that they are extremely stiff when stretched parallel to the layer normal. At a threshold of a few percent strain along the layer normal, the elastomer becomes mechanically softer, and turns opaque [2] because of layer rotation. This behavior is reversible when the strain is removed. Other weakly coupled smectics also have thresholds, but not to layer rotation, and do not have the same extreme mechanical anisotropy [3]. A threshold has also been reported in Sm-*A* materials with a shorter correlation length of the smectic layers, but here the sample remains transparent after the threshold [4]. Typically, smectic elastomers are synthesized in the form of films, either with the layer normal in the plane of the film [1,2,4] or with the layer normal perpendicular to the film plane [5]. However, mechanical testing has only been performed on the first of these two types. The second type would be useful for performing mechanical compression tests parallel to the layer normal.

Experimental study of the electroclinic effect in Sm-*A* elastomers suggests that the layer normal and the director can be manipulated with an electric field and indicates that the two are not necessarily rigidly locked [6], at least on the scale of electrical energies, as a Lagrangian elasticity theory developed in Ref. [7] assumes. Since rubber elastic energies are typically larger than those of electric fields, one would expect mechanical fields also to induce relative rotations. In fact, such relative rotation has been observed experimentally in very recent shear experiments by Kramer and Finkelmann [8].

On the theoretical side, a model of Sm-*A* elastomers has been constructed using nonlinear rubber elasticity extended to smectics [9] that describes the results of Nishikawa and Finkelmann well. This model rigidly locks the director to the layer normal. As mentioned above, a model based on Lagrangian elasticity theory has also been developed [7]. This model fits well with the data, however, unlike [9], it allows in principle for the relative rotation of the director and the layer normal. Triggered by experiments of Kramer and Finkelmann [8,10] where in-plane shears were applied to Sm-*A* elastomers, the rubber elastic approach has been extended [11] very recently to the case of soft anchoring. In Ref. [11], we used this model specifically to study the shear experiments of Kramer and Finkelmann. In the present paper, we employ this model to study various shear and stretch deformations.

The plan of presentation is the following: First, we review the extension of nonlinear rubber elasticity theory to smectics. The fundamental distortions of imposed in-plane stretch and in-plane shear are then explored. Armed with these modes of deformation, we then explore imposed extension and compression along the layer normal which are complex but decomposable into the fundamental modes.

II. MODEL FREE ENERGY

The model free energy reviewed here is generalization of the original rubber elastic model of smectics [9], and was developed originally in Ref. [11]. It has contributions from the background nematic elasticity, and from the compression or dilation of the layers. In addition to these two terms, we include here a potential that penalizes the deviation of the director from the layer normal [12]:

$$f = f_{\text{trace}} + f_{\text{layer}} + f_{\text{tilt}}. \tag{1}$$

The nematic component of the free energy density has been widely discussed [13], and is given by

$$f_{\text{trace}} = \frac{1}{2}\mu \text{Tr}[\underline{\underline{\lambda}} \cdot \underline{\underline{\ell}}_0 \cdot \underline{\underline{\lambda}}^T \cdot \underline{\underline{\ell}}^{-1}], \tag{2}$$

where μ is the isotropic state shear modulus, $\underline{\underline{\lambda}}$ is the deformation gradient tensor, $\underline{\underline{\ell}}_0 = \underline{\underline{\delta}} + (r-1)\mathbf{n}_0\mathbf{n}_0$ is the step-length tensor before the deformation has been applied, $\underline{\underline{\ell}}^{-1} = \underline{\underline{\delta}} + (1/r-1)\mathbf{n}\mathbf{n}$ is the inverse of the step-length tensor after the deformation has been applied, and $\underline{\underline{\delta}}$ is the unit tensor. The step-length tensor is proportional to the second moment of the Gaussian distribution of anisotropic chains making up the rubbery network. The anisotropy of the chains is parameterized by r. The smectic layers embedded in the elastic matrix give rise to the following contribution to the free energy

$$f_{\text{layer}} = \frac{1}{2}B\left(\frac{d}{d_0 \cos \Theta} - 1\right)^2, \tag{3}$$

where B is the layer spacing modulus (typically larger than in liquid smectics), d is the current layer spacing, d_0 is the natural layer spacing, and Θ is the angle between the layer normal and the director. For smectics where the layers are strongly coupled to the matrix, changes in layer spacing can be derived by analyzing how the embedded layer normal deforms in step with the elastic matrix. The layer normal $\mathbf{k}$ and layer spacing are given by [9]

$$\mathbf{k} = \frac{\underline{\underline{\lambda}}^{-T} \cdot \mathbf{k}_0}{|\underline{\underline{\lambda}}^{-T} \cdot \mathbf{k}_0|}; \quad \frac{d}{d_0} = \frac{1}{|\underline{\underline{\lambda}}^{-T} \cdot \mathbf{k}_0|}, \tag{4}$$

where $\mathbf{k}_0$ is the initial layer normal. The deformation of the layer normal outlined above affinely follows that of the rubber matrix because the energetic penalty of not doing so scales with the system size in the microscopic model described in [9]. The $\cos \Theta$ term reflects the projection of the rods making up the layer spacing contracting as the director tilts. Note that this term does not include the finite thickness of the rods, since as $\Theta \to \pi/2$ then $d \to 0$ to avoid a diverging energy penalty, and so the layer thickness tends to zero. However, physically there must be a transition to a constant layer thickness as the angle Θ increases, i.e., there must be forces preventing $\Theta \to \pi/2$ independent of the layer-compression term.

The contribution $f_{\text{tilt}} = f_{\text{tilt}}(\sin \Theta)$ to the free energy density penalizes the deviation of the director from the layer normal. To ensure a finite layer thickness, see the discussion above, the general form of the tilt contribution will be such that $f_{\text{tilt}}(\sin \Theta) \to \infty$ as $\Theta \to \pi/2$. When expanded to leading order in $\sin \Theta$, it reduces to

$$f_{\text{tilt}} = \frac{1}{2}a_t \sin^2 \Theta, \tag{5}$$

where a_t is a coefficient that vanishes as the *A-C* transition is approached. For simplicity, we will work in the following with the simple phenomenological form (5).

Typical values of the constants are $B \sim 10^7$ Pa, $\mu \sim 10^5 - 10^6$ Pa, and $a_t \sim 10^5 - 10^6$ Pa. The value of a_t is estimated from the experiments by Brehmer *et al.* [14], which indicates that $a_t \sim 10^5$ Pa, and Archer and Dierking [15], which produces a value of $a_t \sim 10^6$ Pa. These are results for the liquid state which we expect to be a good estimate for
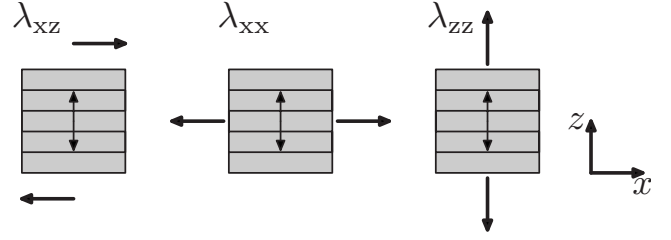

FIG. 1. The imposed shear, in-plane elongation, and out of plane elongation (and compression) geometries that will be considered in this paper.

liquid crystal elastomers since a_t describes a local, molecular property. In determining the main features of the material properties, only the ratios of these values are important. Consequently we will denote

$$b = B/\mu \quad \text{and} \quad c = a_t/\mu. \tag{6}$$

Note that the limit $c \to \infty$ locks the director to the layer normal. On the other hand, when c is small as it would be near the *A-C* transition, deviations of Θ from zero can be large. Dominating these energy scales is that for volume change. The bulk modulus is, as for all rubbers, of the order of 10^9 Pa which means that deformations are at constant volume, that is $\det[\underline{\underline{\lambda}}] = 1$ rigidly.

Note that a semisoft term could also be included of the form

$$f_{\text{semi}} = \frac{1}{2}\alpha\mu \text{Tr}[\underline{\underline{\lambda}} \cdot (\underline{\underline{\delta}} - \mathbf{n}_0\mathbf{n}_0) \cdot \underline{\underline{\lambda}}^T \cdot \mathbf{n}\mathbf{n}]. \tag{7}$$

The value of α can be estimated from either the soft plateau in elastomers, or from the electroclinic effect, and is typically found to be $\alpha < 0.1$. It turns out that this term does not affect the qualitative features of the mechanic response to the deformations that we consider. We will discuss this issue briefly and exemplarily in our analysis of xz shear, but we will not scrutinize the effects of the semisoft term in detail.

III. EXAMPLE GEOMETRIES

Three deformation geometries will be considered here, and are shown in Fig. 1, together with the initial director and layer normal which are assumed to be along $\mathbf{z}$.

The model described above has a complicated form because incompressibility forces the appearance of a cofactor of the deformation gradient $\underline{\underline{\lambda}}$. It is possible to eliminate the cofactor dependence by recognizing that the director and layer normal move in a 2D subspace, which we take to be the xz plane (where $\mathbf{z}$ is parallel to the initial layer normal). Then all the actual calculations can be made using a 2D representation of this model outlined in appendix.

A. Imposed λ_{xz}

First we examine the imposed shear deformation as depicted in Fig. 1. Here the following will be used:

$$\underline{\underline{\lambda}} = \begin{pmatrix} \lambda_{xx} & 0 & \lambda_{xz} \\ 0 & \lambda_{yy} & 0 \\ 0 & 0 & \lambda_{zz} \end{pmatrix}; \quad \begin{aligned} \mathbf{n}_0 &= (0,0,1) \\ \mathbf{n} &= (\sin\theta, 0, \cos\theta). \end{aligned} \quad (8)$$

To ensure incompressible response, $\det(\underline{\underline{\lambda}}) = 1$, one takes $\lambda_{yy} = 1/(\lambda_{xx}\lambda_{zz})$. For this choice of $\underline{\underline{\lambda}}$, the new layer normal is $\underline{\underline{\lambda}}^{-T} \cdot \mathbf{k}_0 = \mathbf{k}_0/\lambda_{zz}$. Layers are unrotated, but generally dilated by λ_{zz}. The deviation of $\mathbf{n}$ from $\mathbf{k}_0$, that is Θ, can thus be identified with the usual θ, the rotation of the director. We use θ until later when there is layer rotation and the distinction must be drawn. On substituting these expressions into the free energy density we obtain the following expression:

$$f = \frac{1}{2}B\left(\frac{\lambda_{zz}}{\cos\theta} - 1\right)^2 + \frac{1}{2}a_t \sin^2\theta$$
$$+ \frac{1}{2}\mu\left(\frac{1}{\lambda_{xx}^2\lambda_{zz}^2} + \lambda_{xx}^2\left[\cos^2\theta + \frac{1}{r}\sin^2\theta\right]\right.$$
$$\left. + (\lambda_{zz}\cos\theta + \lambda_{xz}\sin\theta)^2 + r(\lambda_{zz}\sin\theta - \lambda_{xz}\cos\theta)^2\right). \quad (9)$$

For this $\underline{\underline{\lambda}}$, the additional semisoft term in the free energy is $f_{\text{semi}} = \frac{1}{2}\alpha\mu\lambda_{xx}^2\sin^2\theta$. It does not change the qualitative behavior of the elastomer, so will not be considered here.

This free energy should now be minimized with respect to θ, λ_{xx}, and λ_{zz}. It is straightforward to find the minimal value of λ_{xx}:

$$\lambda_{xx}^4 = \frac{1}{\lambda_{zz}^2\left(\cos^2\theta + \frac{1}{r}\sin^2\theta\right)}. \quad (10)$$

We now assume that B is much larger than a_t and μ so that we can approximate $\lambda_{zz} \approx \cos\theta$. Such an identification is forced by the first term of Eq. (9) when its coefficient is large.

The response for $\lambda_{xz} \ll 1$ will involve a small rotation of the director away from the layer normal, and it can be calculated to leading order by assuming that $\theta \ll 1$ and $\lambda_{zz} \sim 1$. The minimization of Eq. (9) gives (recalling that c is the reduced angular modulus a_t/μ):

$$\theta \approx \frac{(r-1)r\lambda_{xz}}{cr + (r-1)^2}, \quad (11)$$

$$f \approx \frac{3\mu}{2} + \frac{\mu}{2}\frac{cr^2\lambda_{xz}^2}{cr + (r-1)^2}, \quad (12)$$

$$\sigma \approx \mu\frac{cr^2\lambda_{xz}}{cr + (r-1)^2}, \quad (13)$$

where σ is the nominal or engineering stress $\partial f/\partial\lambda_{xz}$. Asymptotic analysis can also be performed for large deformations, but it should be remarked that whilst the assumptions of very large strains seem unrealistic, the results obtained from asymptotic methods are usually applicable to a much larger region than anticipated. Taking $\lambda_{xz} \gg 1$, and $\lambda_{zz} \ll 1$, or equivalently assuming director rotation is now
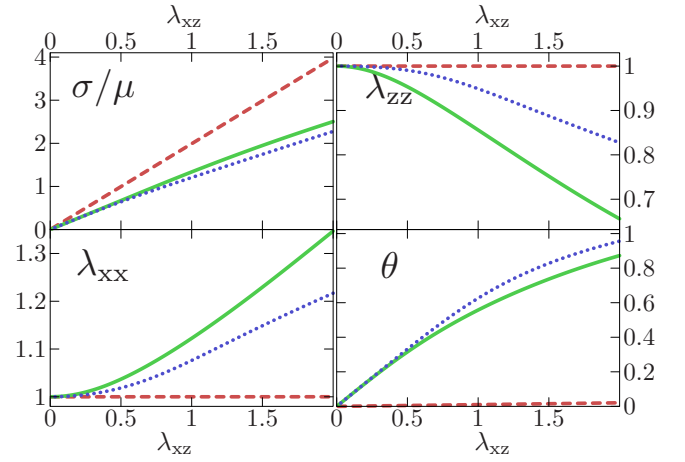

FIG. 2. (Color online) The nominal shear stress, the deformation components λ_{zz} and λ_{xx}, and the rotation angle θ of the director for an imposed λ_{xz} deformation. The dashed (red) line has $(b,c,r) = (60,100,2)$, the solid (green) line has $(60, 1, 2)$, and the dotted (blue) line has $(1, 1, 2)$.

large, $\theta = \pi/2 - \chi$ with χ small, we have to leading order:

$$\lambda_{zz} \approx \frac{1}{(r-1)^{1/3}r^{1/6}\lambda_{xz}^{2/3}}, \quad (14)$$

$$f \approx \frac{\mu}{2}\lambda_{xz}^2, \quad \sigma \approx \mu\lambda_{xz}. \quad (15)$$

Shear across an unmoving director has a modulus $r\mu$, as for instance inspection of Eq. (13) in the $c \gg 1$ limit reveals. Here in this unphysical limit, the modulus has dropped to μ, indicative of minimal chain extension in the gradient direction of the shear. As discussed above, this extreme director rotation is an artifact of the reduction of f_{tilt}, which in its full form has to suppress the approach of Θ to $\pi/2$ on physical grounds.

To illustrate the intermediate features of the model, Fig. 2 shows the numerical solution to the minimization problem, and Fig. 3 shows an illustration of the deformation of the elastomer. Since the xx and zz response is independent of the sign of λ_{xz}, on symmetry grounds for small imposed shear, $\lambda_{xx} - 1 \sim \lambda_{xz}^2$ and $\lambda_{zz} \sim -\lambda_{xz}^2$. Rotation does sense the sign and hence $\theta \sim \lambda_{xz}$. For small values of c, θ saturates at $\pi/2$ for large deformation. By contrast, for large values of c the director rotation is suppressed, in agreement with [9].

In the shear experiments of Kramer and Finkelmann [8,10] the applied deformations are similar to the one that we just discussed. There is, however, the difference that these experiments use setups (tilter and slider) that pre-set λ_{zz} as
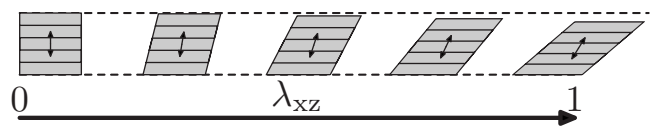

FIG. 3. An illustration of the rotation of the director, and the sympathetic shears for an imposed λ_{xz} deformation, with $(b,c,r) = (60,1,2)$ as on the solid (green) line in Fig. 2.
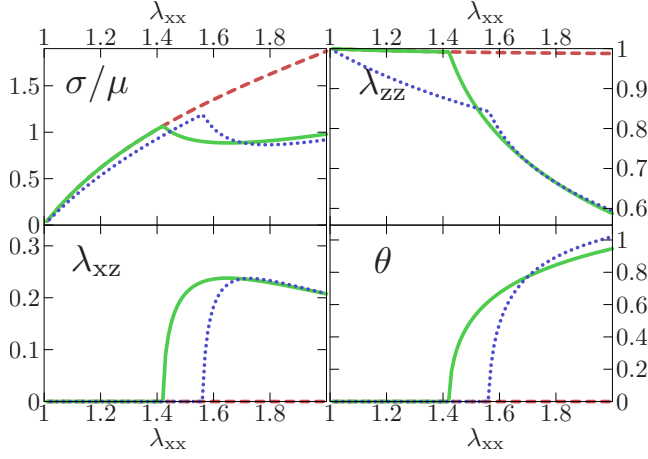
FIG. 4. (Color online) The nominal shear stress, rotation angle, and deformation tensor components for an imposed λ_{xx} deformation. The key is the same as in Fig. 2. Note that $\lambda_{xz} \approx 0$ and $\theta \approx 0$ for $c \gg 1$ [dashed (red) line].

shear proceeds, and hence free relaxation of λ_{zz} as above is not possible. A detailed analysis of these experiments is given in [11].

B. Imposed λ_{xx}

The deformation tensor is still that of Eq. (8), and the free energy takes the same form Eq. (9) as in the previous section. The relaxation behavior of the system is sketched in Fig. 4, which illustrates several interesting features including a threshold at which rotation of the director starts, and a nonmonotonic stress-strain curve.

Analytically it is possible to obtain an expression for the threshold value of λ_{xx} at which the instability starts. Minimization of the free energy in Eq. (9) with respect to λ_{xz} results in the following expression:

$$\lambda_{xz} = \frac{(r-1)\lambda_{zz} \cos \theta \sin \theta}{\sin^2 \theta + r \cos^2 \theta}. \tag{16}$$

We again consider the case where $B \gg a_t, \mu$, and so $\lambda_{zz} \approx \cos \theta$. This leaves only the variable λ_{zz} to be minimized over in the problem. For large B the threshold occurs when there is a minimum at $\lambda_{zz} = 1$, which results in the following condition on λ_c, the critical value of λ_{xx},

$$\lambda_c^4(r-1) - \lambda_c^2(cr-1) - r = 0. \tag{17}$$

Consequently, the threshold is given by

$$\lambda_c^2 = \frac{(cr-1) + \sqrt{4(r-1)r + (cr-1)^2}}{2(r-1)}. \tag{18}$$

This threshold is unphysically large for $c \gg 1$ and so it would be inaccessible to mechanical experiments in this limit. But when $r=2$ and $c=1$, we have $\lambda_c = \sqrt{2}$, in agreement with the numerical results presented in Fig. 4 and possibly within the range of experiments.

The behavior of the system for both small and large values of the deformation can again be analyzed. Before the

threshold, we have $\theta = \lambda_{xz} = 0$, and $\lambda_{zz} = 1$. Consequently

$$f = \frac{1}{2}\mu\left(1 + \lambda_{xx}^2 + \frac{1}{\lambda_{xx}^2}\right), \tag{19}$$

$$\sigma = \mu\left(\lambda_{xx} - \frac{1}{\lambda_{xx}^3}\right), \tag{20}$$

which is the 2D rubber elastic response seen experimentally [2] in the case where the director and layer normal are rigidly anchored, and described theoretically in this framework in [9]. After the threshold we have for $\lambda_{xx} \gg 1$

$$\lambda_{zz} \approx \left(\frac{r}{r-1}\right)^{1/4} \frac{1}{\lambda_{xx}}, \tag{21}$$

$$\theta \approx \pi/2 - \left(\frac{r}{r-1}\right)^{1/4} \frac{1}{\lambda_{xx}}, \tag{22}$$

$$\lambda_{xz} \approx \frac{\sqrt{(r-1)r}}{\lambda_{xx}^2}, \tag{23}$$

$$f \approx \frac{\mu}{2r}\lambda_{xx}^2. \tag{24}$$

This limit is again extreme and unphysical, but useful for understanding trends. The result is the same as that for a nematic rubber that is being stretched perpendicular to its director, the director subsequently rotating to be parallel to the applied elongation, the x direction. The $1/r$ reduction in the effective modulus arises because there is an effective xx elongation of $\sqrt{r}$ on director rotation and the effective extension with respect to this state is only $\lambda_{xx}/\sqrt{r}$.

The induced shear at the threshold $\lambda_{xx} = \lambda_c$ increases infinitely quickly with stretch, as is the case in theory and experiment [16] for the response at the threshold when nematic elastomers are stretched perpendicular to their initial director. A symmetry argument shows that this must be the case: the instability is insensitive to the signs of the angle θ and the shear λ_{xz}, and the stretch λ_{xx} does not distinguish among these signs. Thus one must have $\lambda_{xz}^2 \sim \lambda_{xx} - \lambda_c$ and $\theta^2 \sim \lambda_{xx} - \lambda_c$ (or higher even powers of λ_{xz} and θ). On taking roots, one has $\lambda_{xz} \sim \pm \sqrt{\lambda_{xx} - \lambda_c}$ and $\theta \sim \pm \sqrt{\lambda_{xx} - \lambda_c}$, that is, singular growth at λ_c.

The results here clearly show a nonmonotonic stress-strain relation that is not seen, for instance, in theory or experiment for Sm-A elastomers at their instability under a λ_{zz} extension along their layer normal (see Sec. III C below). In the zz extension case, the layer normal rotates away from the extension direction to allow in-plane stretch and shear. But in rotating away, the layer normal takes the nematic director with it and thus towards the contraction diagonal associated with the shear that is growing in a singular fashion. For prolate chains, this compression along the director of the naturally long dimension of the chain distribution costs additional energy. This is still a lower energy path than that associated with layer extension which would be suffered if layers did not rotate. By contrast here in the case of in-plane stretch, Fig. 5 shows that when director rotation takes place,
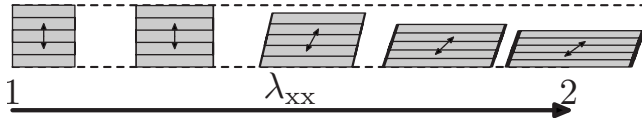
FIG. 5. An illustration of the rotation of the director, and the sympathetic shears for an imposed λ_{xx} deformation, corresponding to the solid (green) line in Fig. 4.

it is instead towards the direction of the *extension* diagonal of the induced xz shear and thus the naturally longer dimension of the chain distribution is more accommodated. This shear grows in a singular fashion. The consequent slow down in the growth of the elastic free energy is sufficient to make the slope of the stress-strain relation negative.

Just as for the van der Waals gas, this type of nonmonotonic stress-strain curve is mechanically unstable to disproportionation. It can be rectified by taking a mixture of the rotated and unrotated states, and making a Maxwell construction on the stress-strain relation. Experimentally, it is expected that there will be a plateau in mechanical behavior that is reversible. This is highly unusual elastic behavior for a solid.

To carry out the Maxwell construction, we define $\hat{f}=f-(\sigma_p\lambda_{xx}+f_0)$, i.e., we subtract from the free energy the common tangent that touches $f(\lambda_{xx})$ at the points of coexisting strain with the same engineering stress σ_p, and we determine σ_p and f_0 such that $\hat{f}$ just touches $\hat{f}=0$ at two points. An illustration of $\hat{f}$ which highlights its nonconvexity is shown in Fig. 6, together with an illustration of the deformation gradient at the two minima. The stress is also shown, with a plateau, that is formed by mixing the two deformation gradients illustrated. The anticipated microstructure may be as illustrated in Fig. 7, however the effects of surface energy and interfacial regions may lead to a different structure. The actual region of the singular shear and director rotation seen in Fig. 4 is thus jumped across and these interesting responses may not be observable.

The value of the threshold provides a useful test for the value of the modulus a_t. As no threshold has been observed through in-plane elongation experiments, it is thought that a_t should be comparable to or larger than μ. For some samples, these stretching experiments have been performed up to a strain of $\lambda_{xx}=2.5$, but no deviation from linearity has been observed [17]. This suggest that the anchoring is so strong in some elastomers, that the sample ruptures before the director and the layer normal become unlocked.
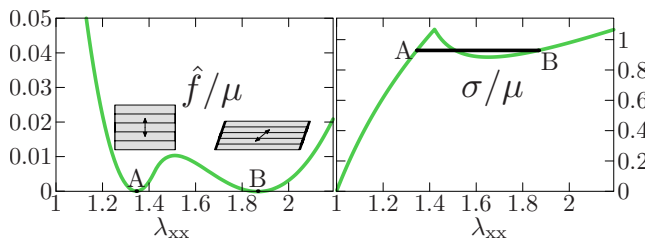

FIG. 6. (Color online) An illustration of the free energy and stress for the nonmonotonic stress strain. The curve illustrated has $(b,c,r)=(60,1,2)$. Here $\lambda_A=1.34$, $\lambda_B=1.87$, and $\sigma_p=0.978\mu$.
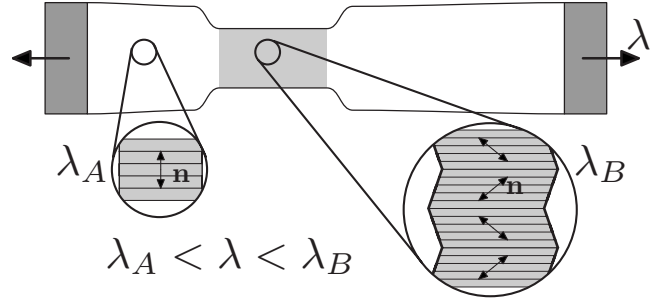

FIG. 7. An illustration of a possible microstructure that would result from the applied in-plane deformation. Depending on the cost of the interface, the disproportionation illustrated here may happen in several regions in the sample. The region where the microstructure forms may be opaque as illustrated.

C. Imposed λ_{zz}

It is well-known that in liquid Sm-*A* [18] and in elastomeric Sm-*A* [2] there is an instability when stretching parallel to the layer normal. For small deformations the elastomer simply elongates, however for large deformations above a threshold, layers start to rotate, and the sample undergoes effective in-plane shear, as first predicted for elastomers within continuum elasticity [19] and previously analyzed in the framework of rubber elasticity [9] but with **n** and **k** rigidly locked ($c=\infty$). When c is finite, elongation parallel to the layer normal still results in the same instability, as is already known from Lagrangian elasticity methods [7]. More unusually, as a consequence of finite c, we predict that compression ($\lambda_{zz}<1$) can also result in a rotational instability, but only of the director with an unrotating layer system.

1. Elongation ($\lambda_{zz}>1$)

Contrary to the deformations considered thus far, elongation along the initial layer normal generates layer rotation, and we are compelled to distinguish between director and layer rotation. Thus we take Θ to denote the angle of the director with respect to the current layer normal, and we introduce ζ as the angle by which the layers rotate relative to the initial layer normal. The deformation gradient tensor

$$\underline{\underline{\lambda}} = \begin{pmatrix} \lambda_{xx} & 0 & 0 \\ 0 & \dfrac{1}{\lambda_{xx}\lambda_{zz}} & 0 \\ \lambda_{zx} & 0 & \lambda_{zz} \end{pmatrix} \tag{25}$$

must be assumed since λ_{zx} shears are those that produce layer rotations, see Eq. (4). This awkward form of the deformation gradient can be decomposed to reveal the true deformations by incorporating a rotation matrix. We first deform the system by $\underline{\underline{\Lambda}}$ which we take to be as in the previous cases, i.e. as in Eq. (8) with stretches and instead an xz shear. The layer normal, given this type of deformation, is as yet unrotated. We then perform a body rotation on both the elastomer and the director, which of course leaves the free energy invariant. The rotation can be chosen to transform the xz shear of $\underline{\underline{\Lambda}}$ into the zx shear of $\underline{\underline{\lambda}}$ in (25). The overall deformation is made up as follows:
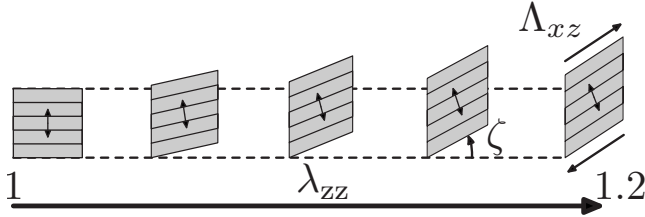
FIG. 8. An illustration of the rotation of the director, and the sympathetic shears for an imposed λ_{zz} elongation. The Λ_{xz} shear is shown in the frame of the layer system. ζ is the shear angle and the rotation angle to go from the lab to the layer frames.

$$\underline{\underline{\lambda}} = \underline{\underline{R}}(\zeta) \cdot \underline{\underline{\Lambda}}; \quad \underline{\underline{\Lambda}} = \begin{pmatrix} \Lambda_{xx} & 0 & \Lambda_{xz} \\ 0 & \Lambda_{yy} & 0 \\ 0 & 0 & \Lambda_{zz} \end{pmatrix}, \quad (26)$$

where $\underline{\underline{R}}(\zeta)$ represents a rotation through an angle ζ about y. At this point we can see that all mechanical deformations of Sm-*A* can be reduced to the three of Fig. 1—others can be reduced to these by suitable rotations.

Figure 8 shows the development of the λ_{ij}, including λ_{zx} in response to λ_{zz}. The last sketch has the Λ_{xz} marked in as it would appear in the frame of the body. The rotation angle ζ can be determined by demanding that the Λ_{zx} component is zero. Practically, this is done by putting in the explicit form for $\underline{\underline{R}}$ in the above, evaluating $\underline{\underline{\Lambda}} = \underline{\underline{R}}^T \cdot \underline{\underline{\lambda}}$ and inspecting Λ_{zx}. It is also clear geometrically from the second to last frame of Fig. 8 that to convert $\underline{\underline{\Lambda}}$ to the lab frame $\underline{\underline{\lambda}}$ one needs to rotate by the shear angle $\zeta = \tan^{-1}(\Lambda_{xz}/\Lambda_{zz})$, resulting in $\cos\zeta = \frac{\Lambda_{zz}}{\sqrt{\Lambda_{xz}^2 + \Lambda_{zz}^2}}$. The connection between the new deformation components Λ_{ij} and the old λ_{ij} is then

$$\lambda_{xx} = \frac{\Lambda_{xx}\Lambda_{zz}}{\sqrt{\Lambda_{xz}^2 + \Lambda_{zz}^2}}, \quad (27)$$

$$\lambda_{zx} = \frac{\Lambda_{xx}\Lambda_{xz}}{\sqrt{\Lambda_{xz}^2 + \Lambda_{zz}^2}}, \quad (28)$$

$$\lambda_{zz} = \sqrt{\Lambda_{xz}^2 + \Lambda_{zz}^2}, \quad (29)$$

see [9] for explicit discussion.

Recall that Θ is the angle between the layer normal and the director. Since the body and the system of layers is rotated by $-\zeta$, the director can be expressed as

$$\mathbf{n} = (\sin[\Theta - \zeta], 0, \cos[\Theta - \zeta]), \quad (30)$$

so that after rotation by ζ in (26) it becomes $\mathbf{n} = (\sin[\Theta], 0, \cos[\Theta])$. After this transformation is performed, we obtain the free energy density again given by Eq. (9) with $\lambda_{ij} \rightarrow \Lambda_{ij}$ and $\theta \rightarrow \Theta$. However, we do not impose Λ_{zz}, but still impose λ_{zz}, whereupon $\Lambda_{zz} = \sqrt{\lambda_{zz}^2 - \Lambda_{xz}^2}$ on rearranging (29). The behavior of the system can be analyzed numerically and results for this analysis are presented in Fig. 9. Note we still see a threshold behavior, but now in addition a rotation of the director with respect to the layer normal Θ. From the decomposition discussed above, it is clear the rotation of the director with respect to the layer normal arises
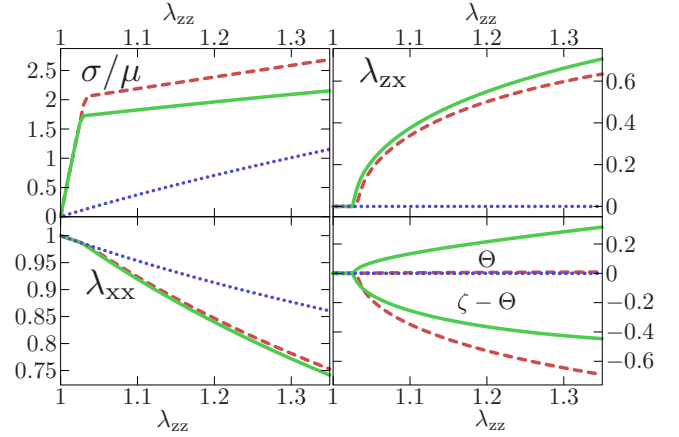

FIG. 9. (Color online) The nominal shear stress, rotation angle, and deformation tensor components for an imposed $\lambda_{zz} > 1$ deformation. The key is as in Fig. 2. Note that the dashed (red) curve for Θ lies above zero for λ_{zz} exceeding the threshold, although this is hard to see because Θ is very small.

because of the effective xz shear. Consequently we expect a nonzero value of Θ on symmetry grounds as observed in Sec. III A.

There are several ways that the position of the threshold can be computed. One method is to expand the free energy density for small values of Θ. We can then minimize with respect to Θ, and substitute in the minimal value. It is then possible to minimize over Λ_{xx}, and substitute this back into the free energy. Only Λ_{xz} remains to be minimized over. Setting the second derivative of this expression with respect to Λ_{xz} to zero at $\Lambda_{xz} = 0$ then gives the equation for the threshold, because it gives the point where the level sets change from being convex to concave. This results in the following polynomial for the critical value λ_c of λ_{zz}:

$$b^2 r(\lambda_c - 1)^2 \lambda_c^4 - b(\lambda_c - 1)\lambda_c^2(2r - 1) - (r - 1)(\lambda_c^3 - 1)$$
$$+ cr\lambda_c[(b - r + 1)\lambda_c^3 - b\lambda_c^2 - 1] = 0. \quad (31)$$

The terms in c have been collected together here, so that it is clear that for $c \gg 1$ the same polynomial in square brackets as in the locked director case [9] is recovered. In that case there was only an instability if the reduced layer spacing modulus was large enough, $b > r - 1$. Now if the director is no longer locked to the layer normal, finite c, then there is naturally an instability for even smaller values of b since the lower energy route of rotation is more accessible if the director can rotate towards the extension diagonal associated with the concomitant shear.

In the limit $B \gg a_t, \mu$ for which λ_c exists,

$$\lambda_c \approx 1 + \frac{2r - cr - 1 + \sqrt{(cr + 1)(4r^2 + cr - 4r + 1)}}{2br}. \quad (32)$$

For $r = 2$ and $b = 60$ we have

$$\lim_{c \to \infty} \lambda_c \approx 1 + \frac{r}{b} \approx 1.033, \quad (33)$$

$$\lim_{c \to 1} \lambda_c \approx 1.028, \tag{34}$$

where the limits have been taken from Eq. (31). Consequently the experimental evaluation of this threshold is not sensitive to the value of c, and does not discriminate between the weak anchoring, and the locked layer normal theories.

For small deformations (before the threshold is reached) we have

$$\lambda_{zx} = \Theta = 0, \tag{35}$$

$$\lambda_{xx} = \frac{1}{\lambda_{zz}}, \tag{36}$$

$$f = \frac{1}{2}B(\lambda_{zz} - 1)^2 + \frac{1}{2}\mu\left(\frac{2}{\lambda_{zz}} + \lambda_{zz}^2\right), \tag{37}$$

which is identical to the locked layer normal case.

Before moving on to compression, we find it worthwhile to compare our results to the available experimental findings and other theoretical predictions. The stress-deformation curves for $B \gg \mu$ are in absolute agreement with the experimental curves by Nishikawa and Finkelmann [1] as well as the theoretical predictions of Refs. [9,7]. The results, or at least their interpretation, differ, however, as far as Θ is concerned. As mentioned above, the rubber-elastic model of Ref. [9] assumes that the layer normal and the director are rigidly locked and thus inevitably produces $\Theta = 0$ for any value of λ_{zz}. From their x-ray data, Nishikawa and Finkelmann conclude that there is no relative tilt between layer normal and the director below and above the threshold. The Lagrangian model of Ref. [7] predicts nonzero but small Θ above the threshold, like in the dashed (red) curve in Fig. 9. Given that the angle-resolution in the experiment of Nishikawa and Finkelmann was of the order of one degree, it is possible that there was Sm-*C* like tilt in the experiment that was too small to detect if Θ followed a curve similar to the dashed (red) curve in Fig. 9. In this case, there is no contradiction between the experimental data and the theoretical findings of Ref. [7] and the present paper.

2. Compression ($\lambda_{zz} < 1$)

For the compression case we again use the free energy expression of Eq. (9) since in the absence of a λ_{zx} there is no layer rotation. Compression along the layer normal is resisted by the layer spacing potential. There is also a nematic rubber elastic penalty for the chain compression. Nematic elastomers in theory and experiment [20] are known to reduce their elastic energy on compression along the director by rotation of the director, thereby presenting a shorter dimension of their chain distribution to the imposed strain. We find an analogous effect here. Numerical results for the compression case are shown in Fig. 10, and illustrated in Fig. 11.

There is again a threshold, λ_c, at which rotation starts in the weak anchoring model. The threshold obeys the following polynomial:
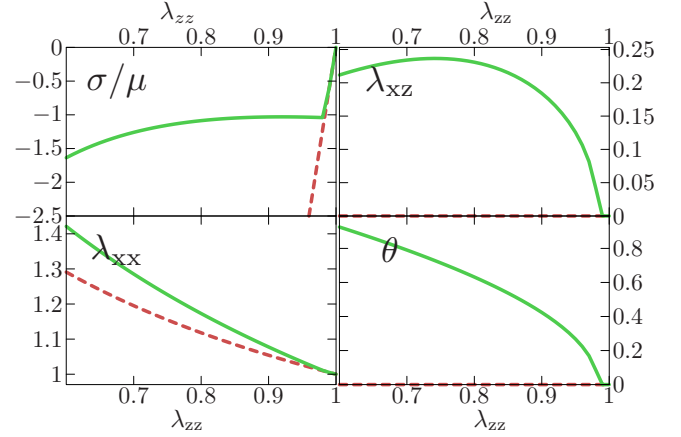

FIG. 10. (Color online) The nominal shear stress, rotation angle, and deformation tensor components for an imposed λ_{zz} deformation. The key is as in Fig. 2. Note that the stress-deformation curve features a slight negative slope that is hard to see.

$$cr\lambda_c + br\lambda_c^2(\lambda_c - 1) + (r - 1)(\lambda_c^3 - 1) = 0. \tag{38}$$

There is always a solution to this equation, that is, in principle an instability against compression should always exist. For $B \gg a_t$, the solution is

$$\lambda_c \approx 1 - a_t/B, \tag{39}$$

which provides an important test for the magnitude of the parameter a_t. For example, if $a_t \sim \mu$ and $B \sim 60\mu$, then $\lambda_c \approx 0.983$, i.e. a compression of a few percent. For large c the instability moves to (unphysically) large compressions, $\lambda_c \sim 0$. At small deformations, before any rotational instability, the behavior is exactly as in the elongation case, given in Eq. (37).

The stress-deformation curve shown in Fig. 10 is again nonmonotonic, so is unstable in the region of negative slope. This unphysical feature can be resolved by resorting to a Maxwell construction as explained in Sec. III B. As in Sec. III B, this construction leads to the prediction of a plateau in the stress-deformation curve and microstructure that features, unless boundary conditions prevent this, a mixture of sheared and compressed regions.

Reference [7] focused on stretching along the layer normal as in the experiments of Nishikawa and Finkelmann, and its authors chose not to consider compression along the layer normal. However, from the equations of Sec. III of Ref. [7], it is straightforward to see that the Lagrangian model also predicts an instability towards shear for compression along the layer, $u_{zz} < 0$, where $\underline{u} = \frac{1}{2}(\underline{\lambda}^T\underline{\lambda} - \underline{\delta})$ is the usual strain tensor. The thresholds u_{zz}^c for the onset of u_{xz} shear are deter-
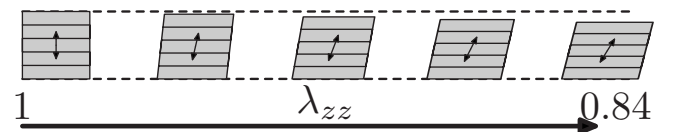

FIG. 11. An illustration of the rotation of the director, and the sympathetic shears for an imposed $\lambda_{zz} < 1$ compression.

mined by the values of u_{zz} for which the effective modulus $r_R(u_{zz})$ in the tilt energy density passes through zero from positive to negative. For the precise definition of the effective modulus, which is related to the parameter a_t defined via Eq. (5), we refer to Eq. (3.10b) of Ref. [7]. The equation $r_R(u_{zz})=0$ has 2 solutions, the one given in Eq. (3.11) of Ref. [7], and a corresponding one with the minus in front of the square root replaced by a plus. The solution with the plus pertains to compression and was, therefore, not discussed in Ref. [7]. Based on the available experimental data for fluid [15] and elastomeric smectics [14], the Lagrangian theory of Ref. [7] produces the estimates $u_{zz}^c \approx -0.025$ and $u_{zz}^c \approx -0.0025$, respectively, which are consistent with estimates for λ_c based Eq. (39) and the typical values for a_t and B quoted in Sec. II.

IV. DISCUSSION AND CONCLUSION

We have explored the consequences of having a weakly anchored director in a model of a Sm-*A* elastomer for three deformations: in-plane shear, in-plane elongation, and deformation parallel to the layer normal. For the in-plane shear, it is found that the director rotates toward the extension diagonal and that initially the rotation angle is proportional to the amplitude of the shear applied. For in-plane elongation, and for compression and elongation parallel to the layer normal, the possibility of rotation of the director leads to the prediction of instabilities of the system to director rotation.

The stress-deformation curves predicted by our model for in-plane elongation and for compression parallel to the layer normal are nonmonotonic. Since a region of negative slope in the stress-deformation curve is unstable, this behavior is unphysical and will not be seen experimentally. Instead the elastomer should form a mixture of two different deformations, and exhibit a plateau in the stress-deformation curve, as illustrated in Sec. III B. In the case of imposed in-plane elongation, disproportionation has not been reported experimentally; it may, however, be possible to engineer elastomers in which this behavior could be observed.

The instability toward the development of shear for elongation along the layer normal has been discussed theoretically in earlier papers [7,9]. Here, we also predict an instability to rotation of the director under compression along the layer normal. This could be analyzed experimentally using the samples in which the director and layer normal are parallel to the normal to the film as reported in [5]. The thresholds at which the different instabilities occur provide a useful way to determine the model parameters experimentally, and to find the value of the parameter a_t.

APPENDIX: GENERAL 2D MODEL FORMULATION

We give here a practical method of calculating the free energy in the complex situations of extensions, shears and rotation. Simplification is possible because the deformations occur in the xz subspace of $\underline{\underline{\lambda}}$ and are denoted by

$$\underline{\underline{G}} = \begin{pmatrix} \lambda_{xx} & \lambda_{xz} \\ \lambda_{zx} & \lambda_{zz} \end{pmatrix}, \tag{A.1}$$

with a single y deformation ($\lambda_{yy} = \det[\underline{\underline{G}}]^{-1}$) that acts to preserve volume. Using this notation, and assuming that the director $\mathbf{n}$ remains in the xz plane, then the nematic free energy density is

$$f_{el} = \frac{1}{2}\mu\{\mathrm{Tr}[\underline{\underline{G}} \cdot \underline{\underline{\ell}}_0 \cdot \underline{\underline{G}}^T \cdot \underline{\underline{\ell}}^{-1}] + (\det \underline{\underline{G}})^{-2}\}. \tag{A.2}$$

The layer normal can be calculated [9] as follows:

$$\mathbf{k} \propto \underline{\underline{\lambda}}^{-T} \cdot \mathbf{z} = (\underline{\underline{\lambda}} \cdot \mathbf{x})(\times \underline{\underline{\lambda}} \cdot \mathbf{y}) = \frac{(\underline{\underline{G}} \cdot \mathbf{x}) \times \mathbf{y}}{\det \underline{\underline{G}}}, \tag{A.3}$$

$$|\underline{\underline{\lambda}}^{-T} \cdot \mathbf{z}| = \frac{|\underline{\underline{G}} \cdot \mathbf{x}|}{\det \underline{\underline{G}}}. \tag{A.4}$$

The last term we require is the dot product of $\mathbf{n}$ and $\mathbf{k}$ to calculate the angle between the layer normal and director.

$$\mathbf{n} \cdot \mathbf{k} = \frac{[(\underline{\underline{G}} \cdot \mathbf{x}) \times \mathbf{y}] \cdot \mathbf{n}}{\underline{\underline{G}} \cdot \mathbf{x} \times \mathbf{y}} = \frac{\sqrt{[\mathbf{n} \times (\underline{\underline{G}} \cdot \mathbf{x})] \cdot [\mathbf{n} \times (\underline{\underline{G}} \cdot \mathbf{x})]}}{|\underline{\underline{G}} \cdot \mathbf{x}|}$$
$$= [1 - (\mathbf{n} \cdot \widehat{\underline{\underline{G}}\mathbf{x}})^2]^{1/2}, \tag{A.5}$$

where $\widehat{\underline{\underline{G}}\mathbf{x}}$ denotes the unit vector $\underline{\underline{G}}\mathbf{x}/|\underline{\underline{G}}\mathbf{x}|$. Combining the above results produces the following total free energy density expression:

$$f = \frac{1}{2}\mu\left\{\mathrm{Tr}[\underline{\underline{G}} \cdot \underline{\underline{\ell}}_0 \cdot \underline{\underline{G}}^T \cdot \underline{\underline{\ell}}^{-1}] + \frac{1}{(\det \underline{\underline{G}})^2}\right\}$$
$$+ \frac{1}{2}B(\det \underline{\underline{G}}/[|\underline{\underline{G}} \cdot \mathbf{x}|^2 - (\mathbf{n} \cdot \underline{\underline{G}} \cdot \mathbf{x})^2]^{1/2} - 1)^2 + \frac{1}{2}a_t(\mathbf{n} \cdot \widehat{\underline{\underline{G}}\mathbf{x}})^2. \tag{A.6}$$

This expression no longer involves the cofactor of the deformation gradient.

[1] E. Nishikawa and H. Finkelmann, Macromol. Chem. Phys. **198**, 2531 (1997).

[2] E. Nishikawa and H. Finkelmann, Macromol. Chem. Phys. **200**, 312 (1999).

[3] P. Beyer, E. M. Terentjev, and R. Zentel, Macromol. Rapid Commun. **28**, 1485 (2007).

[4] A. Komp and H. Finkelmann, Macromol. Rapid Commun. **28**, 1 (2007).

[5] E. Nishikawa, J. Yamamoto, H. Yokoyama, and H. Finkelmann, Macromol. Rapid Commun. **25**, 611 (2004).

[6] C. M. Spillmann, B. R. Ratna, and J. Naciri, Appl. Phys. Lett. **90**, 021911 (2007).

[7] O. Stenull and T. C. Lubensky, Phys. Rev. E **76**, 011706 (2007).

[8] D. Kramer and H. Finkelmann, Phys. Rev. E (to be published).

[9] J. M. Adams and M. Warner, Phys. Rev. E **71**, 021708 (2005).

[10] D. Kramer and H. Finkelmann, e-print arXiv:0708.2024.

[11] O. Stenull, T. C. Lubensky, J. M. Adams, and M. Warner, Phys. Rev. E (to be published).

[12] J.-H. Chen and T. C. Lubensky, Phys. Rev. A **14**, 1202 (1976).

[13] M. Warner and E. M. Terentjev, *Liquid Crystal Elastomers*, 2nd ed. (Oxford University Press, Oxford, 2007).

[14] M. Brehmer, R. Zentel, F. Gieselmann, R. Germer, and P. Zungenmaier, Liq. Cryst. **21**, 589 (1996).

[15] P. Archer and I. Dierking, Phys. Rev. E **72**, 041713 (2005).

[16] H. Finkelmann, I. M. Kundler, E. M. Terentjev, and M. Warner, J. Phys. II **7**, 1059 (1997).

[17] D. Kramer (private communication).

[18] N. A. Clark and R. B. Meyer, Appl. Phys. Lett. **22**, 493 (1973).

[19] E. M. Terentjev and M. Warner, J. Phys. II **4**, 111 (1994).

[20] R. Verduzco, G. Meng, J. A. Kornfield, and R. B. Meyer, Phys. Rev. Lett. **96**, 147802 (2006).